ACS APPLIED MATERIALS & INTERFACES

Research Article

www.acsami.org

Direct Observation of Antisite Defects in $LiCoPO_4$ Cathode Materials by Annular Dark- and Bright-Field Electron Microscopy

Quang Duc Truong,* Murukanahally Kempaiah Devaraju, Takaaki Tomai, and Itaru Honma*

Institute of Multidisciplinary Research for Advanced Materials, Tohoku University, Sendai 980-8577, Japan

Supporting Information

ABSTRACT: $LiCoPO_4$ cathode materials have been synthesized by a sol−gel route. X-ray diffraction analysis confirmed that $LiCoPO_4$ was well-crystallized in an orthorhombic structure in the *Pmna* space group. From the high-resolution transmission electron microscopy (HR-TEM) image, the lattice fringes of {001} and {100} are well-resolved. The HR-TEM image and selected area electron diffraction pattern reveal the highly crystalline nature of $LiCoPO_4$ having an ordered olivine structure. The atom-by-atom structure of $LiCoPO_4$ olivine has been observed, for the first time, using high-angle annular dark-field (HAADF) and annual bright-field scanning transmission electron microscopy. We observed the bright contrast in Li columns in the HAADF images and strong contrast in the ABF images, directly indicating the antisite exchange defects in which Co atoms partly occupy the Li sites. The $LiCoPO_4$ cathode materials delivered an initial discharge capacity of 117 mAh/g at a C/10 rate with moderate cyclic performance. The discharge profile of $LiCoPO_4$ shows a plateau at 4.75 V, revealing its importance as a potentially high-voltage cathode. The direct visualization of atom-by-atom structure in this work represents important information for the understanding of the structure of the active cathode materials for Li-ion batteries.

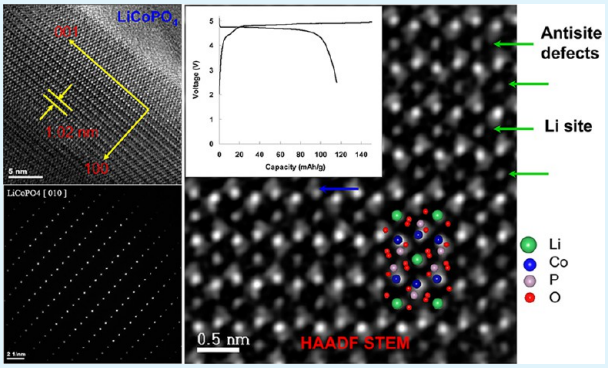

KEYWORDS: *lithium-ion batteries, $LiCoPO_4$, HAADF, ABF, scanning transmission electron microscopy, antisite defects*

1. INTRODUCTION

The development of energy storage systems is critical for addressing the problems of climate change and the shortage of fossils fuels and also plays a key role in the development of renewable energy. Lithium-ion batteries offer promising opportunities for novel energy storage systems and future applications in hybrid electric vehicles (HEVs) or electric vehicles (EVs). To realize the application of lithium-ion batteries suitable for a large scale, the main challenges, namely, energy densities and power densities, have to be optimized.[1,2] One way to improve energy density is to use cathodes having a high redox potential. For this reason, the lithium cobalt phosphates ($LiCoPO_4$) have attracted attention because they offer both flat high potential (at approximately 4.8 V vs Li^+/Li) and good theoretical capacity (167 mAh/g).[3,4] Recently, researchers have focused on improving the electrochemical performance of $LiCoPO_4$ by tailoring the composition, particle morphology, and carbon coating.[5−14] Enhanced cyclic performance has been observed by partial substitution of Co or Li in $LiCoPO_4$ with Fe, V, or another divalent cation.[15−19]

The cyclic performance and rate capacity of a cathode material critically depend on the structural changes and phase transitions taking place during the charge−discharge cycle. Therefore, direct observation of crystal structures, especially structural defects and light elements such as Li, at atomic-level resolution is particularly important for elucidating their charge−discharge behavior and capacity fading. Attempts have been made to analyze the atom-by-atom structure of cathode materials using a scanning transmission electron microscope. For example, Kikkawa et al. observed extraction and insertion of Li in $Li_{1.2}Mn_{0.4}Fe_{0.4}O_2$ using a scanning transmission electron microscope, but only at a low magnification based on electron energy loss spectroscopy (EELS) mapping.[20,21] Li sites in olivine-structured $LiFePO_4$ have also been visualized on an atomic scale with an annular dark-field detector.[22−24] Ikuhara et al. observed the antisite exchange defects, i.e., disordered occupations of Li sites by Fe atoms, providing insight into defect configuration.[22−24] In 2009, an annular bright-field detector was developed for real-time imaging of light elements.[25−27] After that, the same group reported, for the first time, the direct observation of Li and O atoms in oxide spinel nanoparticles of $LiMn_2O_4$ and $LiCoO_2$ using a spherical aberration (Cs)-corrected scanning transmission electron microscopy (STEM) with a newly developed annual bright-field detector.[28,29] However, the signal-to noise ratio is still low. Until recently, Gu et al. could observe Li ions in $LiFePO_4$ and $LiCoO_2$ with good signal-to-noise ratios to reveal the transportation mechanism of Li inside these cathode materials and other anode materials ($Li_4Ti_5O_{12}$ and $TiNb_2O_7$)

Received: May 14, 2013
Accepted: September 23, 2013
Published: September 23, 2013

 © 2013 American Chemical Society dx.doi.org/10.1021/am403018n | ACS Appl. Mater. Interfaces 2013, 5, 9926−9932

during the charge−discharge cycle.[30−34] Clearly, reliably imaging the atom-by-atom structure at atomic resolution is particularly important for elucidating the charge−discharge behavior of cathode materials.

In previous work, we have determined the crystal structure of Li_2CoSiO_4 cathode materials using high-angle annular dark-field (HAADF) and annual bright-field (ABF) STEM.[35] In this paper, we report the synthesis, characterization, and investigation of the atom-by-atom structure of $LiCoPO_4$ olivine particles, for the first time, using spherical aberration-corrected STEM with the visualization of exchange antisite defects at Li atomic sites. Such antisite defects strongly affect the electrochemical performance of the cathode material. In particular, the $LiCoPO_4$ material was used as a cathode material for lithium-ion batteries, and an initial discharge capacity of 117 mAh/g at a C/10 rate (70% of theoretical capacity) was obtained with moderate cyclic performance.

2. EXPERIMENTAL SECTION

$LiCoPO_4$ materials were directly synthesized by a facile sol−gel method with a simple treatment in an air atmosphere. Typically, $LiNO_3$, $Co(NO_3)_2$, $NH_4H_2PO_4$, and citric acid ($C_6H_8O_7$) in a 1:1:1:1 molar ratio were dissolved in distilled water. After complete dissolution of starting materials, the obtained solution was heated while being continuously stirred at 80 °C for 2 h, and then the hot plate temperature was set to 120 °C. After reaction for 12 h, a gel-like specimen resin was obtained. For the pretreatment of samples, the gel-like matter was subjected to pyrolysis at 350 °C for 2 h in an air atmosphere. The resulting carbonate precursor was calcinated at 500 °C for 5 h in air, and the $LiCoPO_4$ particles were obtained. The synthesis condition described above has been optimized to obtain the $LiCoPO_4$ particles providing good cathode performance.

The crystalline phases of the samples were characterized using powder X-ray diffraction (XRD) (Rigaku RINV-2200, 40 kV and 30 mA) with Cu Kα radiation (λ = 1.5406 Å). Data were collected in the 2θ–θ scanning mode with a scan speed of 4°/min and a step size of 0.02°. The morphology of particles was observed using a field-emission scanning electron microscope (Hitachi S-4800 with EDS) at an accelerating voltage of 5 kV. HAADF images, ABF images, elemental mapping, and energy dispersive spectroscopy (EDS) were collected using a JEOL JEM-2100F instrument equipped with a spherical aberration corrector (CEOS). The camera length was 6 cm; the BF aperture was 3 cm, and HAADF and ABF detectors spanned the ranges of 70−180 and 12−24 mrad, respectively.

The electrochemical performance of $LiCoPO_4$ was investigated using cointype cells (CR2032). The working electrode is composed of 80 wt % $LiCoPO_4$, 10 wt % PTFE [poly(tetrafluoroethylene)] as a binder, and 10 wt % acetylene black. These materials were ground with a conventional agar motor to make electrode paste. The prepared paste was spread uniformly, rolled into a sheet, and then dried in a vacuum oven for 4 h at 160 °C. The cathode sheet was punched into circular discs and cut into wafers (7 mm in diameter, 0.025 mm in thickness, 5−6 mg). The tested cell was assembled inside an argon-filled glovebox. For electrochemical measurements, the cell was composed of a lithium metal counter, reference electrodes, and a $LiCoPO_4$ positive electrode. The cathode and reference electrodes were separated by a microporous polypropylene film. A 1 M solution of $LiPF_6$ in a mixed solvent of ethylene carbonate (EC) and dimethyl carbonate (DMC) with a 1:1 volume ratio (Tomiyama Pure Chemical Co., Ltd.) was used as the electrolyte. Charge−discharge cycling was performed galvanostatically between 2.5 and 5.1 V versus Li^+/Li on multichannel battery testers (Hokuto Denko) at various charge−discharge rates ranging from 0.1 to 1 C (1 C = 167 mAh/g). Current densities and specific capacities were calculated on the basis of the weight of the $LiCoPO_4$ cathode in the electrode.

3. RESULTS AND DISCUSSION

3.1. Characterization of the Material. The XRD pattern of the synthesized $LiCoPO_4$ particle is shown in Figure 1. All

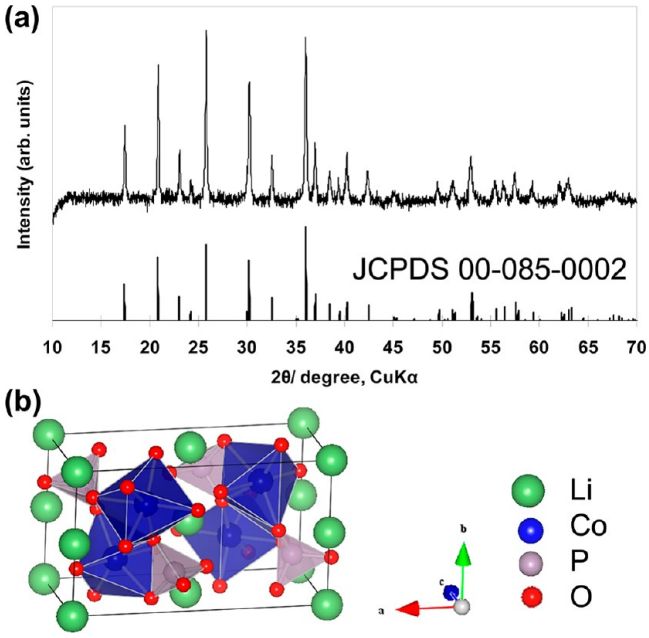

Figure 1. (a) XRD pattern of the synthesized $LiCoPO_4$ particles. (b) Crystal structure of $LiCoPO_4$.

diffraction peaks were indexed to the orthorhombic *Pnma* space group with the following dimensions (in agreement with reported values): a = 10.2045 Å, b = 5.9213 Å, and c = 4.7002 Å.[13,14,36−40] It is evident from the XRD pattern that a single phase of $LiCoPO_4$ with an olivine structure has been prepared.

The particle morphology was observed using high-resolution transmission electron microscopy (HR-TEM). The $LiCoPO_4$ particles show diameters ranging from 100 to 300 nm evidenced by TEM images (Figure 2a,b). Panels c−e of Figure 2 show the HR-TEM images and the selected area electron diffraction (SAED) pattern of a typical particle. The SAED pattern taken from the particles can be indexed to the [010] zone axis of single-crystal olivine structure, indicating that the particle is single-crystalline in nature (Figure 2e). The HR-TEM images in panels c and d of Figure 2 clearly show the interplanar spacing of (100) and (001) atomic planes. The lattice fringe spacing is 1.02 nm along the [100] direction, which is consistent with the unit cell parameter along the crystallographic a direction (a = 10.2045 Å). A corresponding model of atomic arrangement of the $LiCoPO_4$ olivine structure projected along the [010] direction is displayed in Figure 2f, which is in agreement with the observation shown in panels d and e of Figure 2. More importantly, the lattice fringes are aligned without any dislocation, and the diffraction spots are uniform, indicating the high crystallinity of the obtained structures.

Compared to the well-known $LiFePO_4$ material, the $LiCoPO_4$ material and its crystal structure have been studied less. The structure is composed of a chain of distorted CoO_6 octahedra, each octahedron cross-linked with a PO_4 tetrahedral oxo-anion by either corner sharing or edge sharing (Figure 1b). The [010] projection of $LiCoPO_4$ with separated aligned columns of Li, Co, and P ions is most suitable for observing these ions (Figure 3a). Six Co columns form with each other a hexagon configuration,

dx.doi.org/10.1021/am403018n | ACS Appl. Mater. Interfaces 2013, 5, 9926−9932

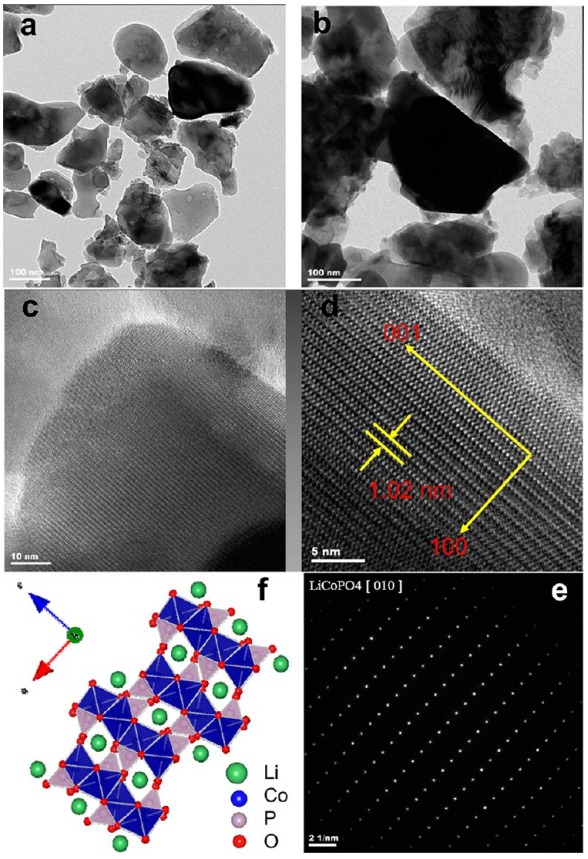

Figure 2. (a and b) TEM images at different magnifications. (c and d) HR-TEM images at different magnifications of the particle shown in panel b. (e) ED pattern of the synthesized $LiCoPO_4$ particles. (f) Crystal structure of $LiCoPO_4$ viewed along the [010] direction.

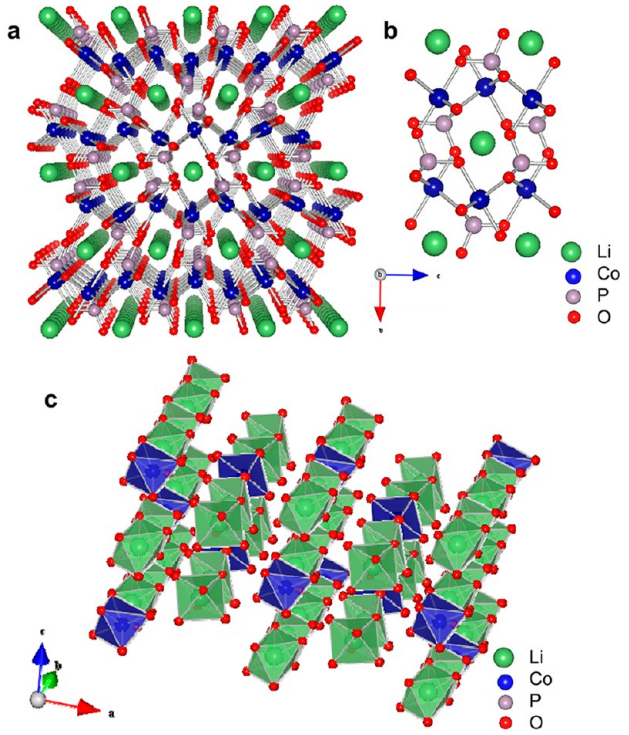

Figure 3. Schematic illustrations of (a) the $LiCoPO_4$ olivine structure, (b) a unit cell, and (c) the homogeneous distribution of the antisite exchange Co atoms at M1 Li sites of $LiCoPO_4$.

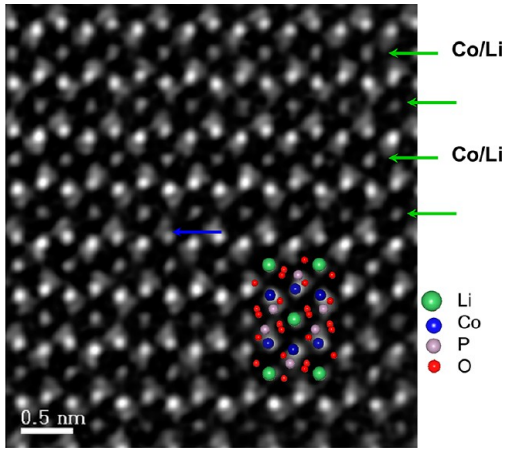

Figure 4. HAADF STEM image of the $LiCoPO_4$ particle viewed along the [010] direction. The superimposed atomic arrays in the inset indicate the locations of atom columns. The blue arrow indicates the Co column with weak contrast.

and each Co column is accompanied by a P column (Figure 3b). Li is located at edge-sharing M1 sites, and Co is found in the corner-sharing M2 sites. It has been confirmed by theoretical calculation and experimental observation that cation exchange antisite defects between two octahedral M sites are the most frequently occurring point defects in the olivine structure.[22−24,41−46]

Figure 4 shows an HAADF STEM image viewed along the [010] direction of a $LiCoPO_4$ particle. The two-dimensional atomic arrangement of a unit cell is superimposed on the image for comparison. The Co sites can be clearly seen as the brightest contrast in Figure 4. The P sites are located near each Co site. Six Co columns form with each other a hexagon configuration that matches well the illustration in Figure 3b. The O columns, however, are not well resolved from Co and P columns because of the overlapping of these three atomic columns viewed along the [010] projection, which is in good agreement with the observation of the $LiFePO_4$ structure by Ikuhara et al.[30] Because the ADF image contrast roughly correlates with the atomic number according to a $Z^{1.7}$ relationship,[30,31] Li atoms ($Z = 3$) are invisible even at the high resolution of the HAADF mode.[22−31] The image simulation based on the multislice method and experimental observation of olivine structure by HAADF STEM also confirmed that no visible contrast is found in the Li columns.[22−24] Therefore, strong contrast visualized in the Li sites in Figure 4 indicates that Li sites have been occupied by Co atoms (Figure 3c). The strong and uniform contrasts observed in Li columns suggest that Li-to-Co exchange antisite defects in $LiCoPO_4$ are intensive and homogeneously distributed in the lattice, which differs from the case in $LiFePO_4$ or $LiMnPO_4$ structures.[22,24] Moreover, HAADF images were taken from different particles with a total of 500 lithium columns in the [010] direction; all of them are visible in the image with a good signal-to-noise. To further confirm the Li-to-Co exchange, we critically observed the HAADF image to find Co columns with a slightly bright contrast. As shown in Figure 4 (blue arrow), the weak contrast of a Co column is found, presumably resulting from the cation exchange by light Li atoms. Thus, the crystallographic disorder in $LiCoPO_4$ is an antisite defect rather than an excess of Co.

dx.doi.org/10.1021/am403018n | ACS Appl. Mater. Interfaces 2013, 5, 9926−9932

Figure 5a shows an annular bright-field STEM image viewed along the [010] direction of $LiCoPO_4$. Similarly, the Co and P

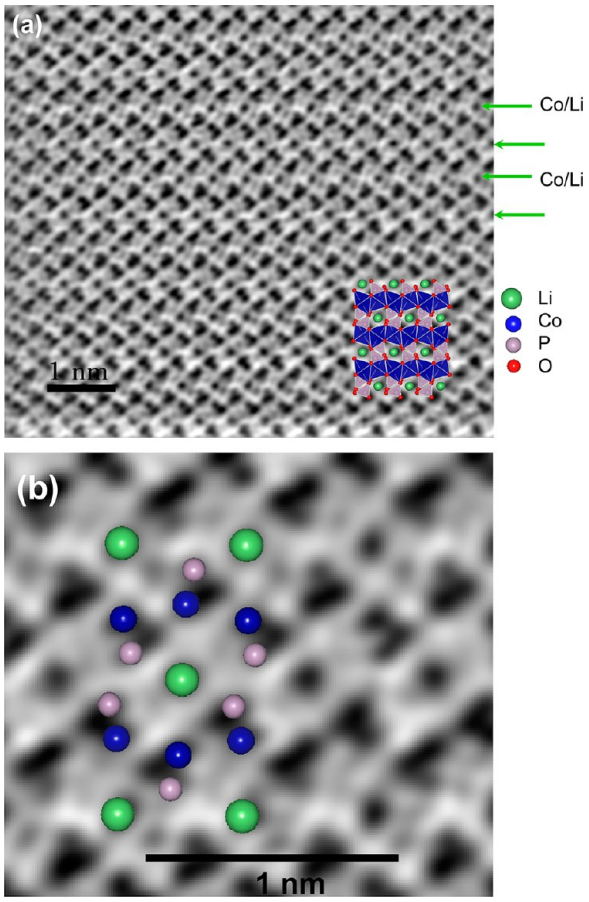

Figure 5. (a) ABF STEM image viewed along the [010] direction. (b) Enlarged ABF STEM image of the synthesized $LiCoPO_4$ particle. The superimposed atomic arrays in each image indicate the locations of atom columns. The inset in panel a shows an illustration of the olivine $LiCoPO_4$ structure viewed along the [010] direction.

atomic columns can be directly visualized by comparing them with the corresponding structure schematically shown in the inset of Figure 5b. Because Li is very light, the signals of Li columns should be weak because of the atomic number *Z*-dependent property of contrast (*Z* contrast).[28−31] However, the intensity of the Li columns in this case is very strong, even comparable to that of Co columns (Figure 5b), suggesting that Co atoms reside at Li sites. The direct visualization of Li columns in this case, however, is difficult because of the intensive antisite exchange defects.

The computational models and first-principle methods of the orthorhombic olivine $LiMPO_4$ structure indicated that the Li^+ diffusion energy is orientation-dependent and is lowest for the pathway along the the [010] channel.[47] The movement of Li ions in the *b* direction at the phase boundary has also been observed by electron microscopy[48] or by combining high-temperature powder neutron diffraction and the maximum entropy method.[49] Thus, it is accepted that lithium ions one-dimensionally diffuse along the *b* axis during the charge−discharge process. The occupation of Li sites by Co cations in a homogeneous configuration unexpectedly blocks the transport of lithium in the *b* direction. This finding explains the low discharge capacity of $LiCoPO_4$ synthesized at temperatures as low as 500 °C. Attempts have been made to improve the discharge capacity of $LiCoPO_4$; however, only 70−80% of the theoretical capacity was obtained.[10−18] This may due to the fact that the antisite defects are profound among the olivine cathode materials synthesized at low temperatures.[50−52]

Furthermore, to verify that the bright contrast of Li columns does not arise form doping element, EDS analysis and elemental mapping of the $LiCoPO_4$ sample by STEM were conducted. EDS elemental mappings by STEM (Figure 6b−d) showed a uniform distribution of Co, P, and O, and the EDS spectrum of the sample exhibits characteristic peaks of Co, P, and O, consistent with the purity of the $LiCoPO_4$ phase determined by XRD and electron microscopy. No other element was detected in EDS analysis by STEM. These characterizations confirm the purity, homogeneity, and uniform elemental distribution in the obtained particles. The synthetic method includes citric acid as a complexing agent; thus, it is expected that amorphous C was coated *in situ* on the synthesized particles. In particular, the presence of C was confirmed by EDS (elemental mapping, SEM) (Figure S1 of the Supporting Information) and C was well-distributed beside Co, P, and O. The carbon content of the synthesized material determined by EDS was ∼6.5 atom % (Table S1 of the Supporting Information). A coating of C on the cathode materials has been found to enhance the cyclic performance and rate capacity of $LiCoPO_4$ materials.[13,14,16]

3.2. Electrochemical Performance. The electrochemical performance of the synthesized $LiCoPO_4$ has been measured by the galvanostatic charge−discharge method, and the results are shown in Figure 7. $LiCoPO_4$ exhibited a wide and flat voltage voltage at ∼4.75 V versus Li^+/Li with an initial discharge capacity of 117 mAh/g at a C/10 rate. The sample possesses two voltage plateaus, indicating two-step lithium deintercalation. The cyclic voltammograms of the cell containing $LiCoPO_4$ show two oxidation peaks at 4.8 and 4.9 V versus Li^+/Li and one reduction peak at 4.65 V in agreement with cyclic voltammograms reported by other groups (Figure S2 of the Supporting Information).[53−55] This two-step behavior of the extraction of lithium from $LiCoPO_4$ was associated with the $LiCoPO_4 \leftrightarrow Li_{0.7}CoPO_4$ and $Li_{0.7}CoPO_4 \leftrightarrow CoPO_4$ transitions.[13,55] The low discharge capacity of the obtained material is reasonable because of the presence of antisite defects. The partial occupation of Li sites by Co atoms inevitably blocks the lithium-ion diffusion pathway. The discharge capacity of $LiCoPO_4$ is 57 mAh/g at a 20 cycle with a current rate of 0.1 C, and the retention capacity is ∼49%. $LiCoPO_4$ cathodes have generally suffered from poor cycling stability.[55] It was also demonstrated that the capacity fading of $LiCoPO_4$ is due to the instability of the electrolyte at 5 V. The side reactions between the electrolyte and electrode may produce a solid−electrolyte interface (SEI), leading to oxidation of the electrolyte and loss of lithium.[14] Figure 7c presents the rate capacity of the cells containing $LiCoPO_4$ at various discharge rates ranging from 0.1 to 1 C. The cell exhibited a first discharge capacity of 117, 93, 80, and 67 mAh/g at 0.1, 0.2, 0.5, and 1 C, respectively. At a high discharge rate of 0.5−1 C, the cell exhibited a reduced discharge plateau at 4.5−4.4 V due to the instability of the electrolyte and the formation of an SEI.

4. CONCLUSIONS

$LiCoPO_4$ has been successfully prepared by a modified sol−gel method. The XRD pattern of $LiCoPO_4$ particles could be identified as a single phase of olivine structure indexed by the orthorhombic *Pmna* space group. The calculated lattice parameters agreed well with the reported data. It could also be

dx.doi.org/10.1021/am403018n | ACS Appl. Mater. Interfaces 2013, 5, 9926−9932

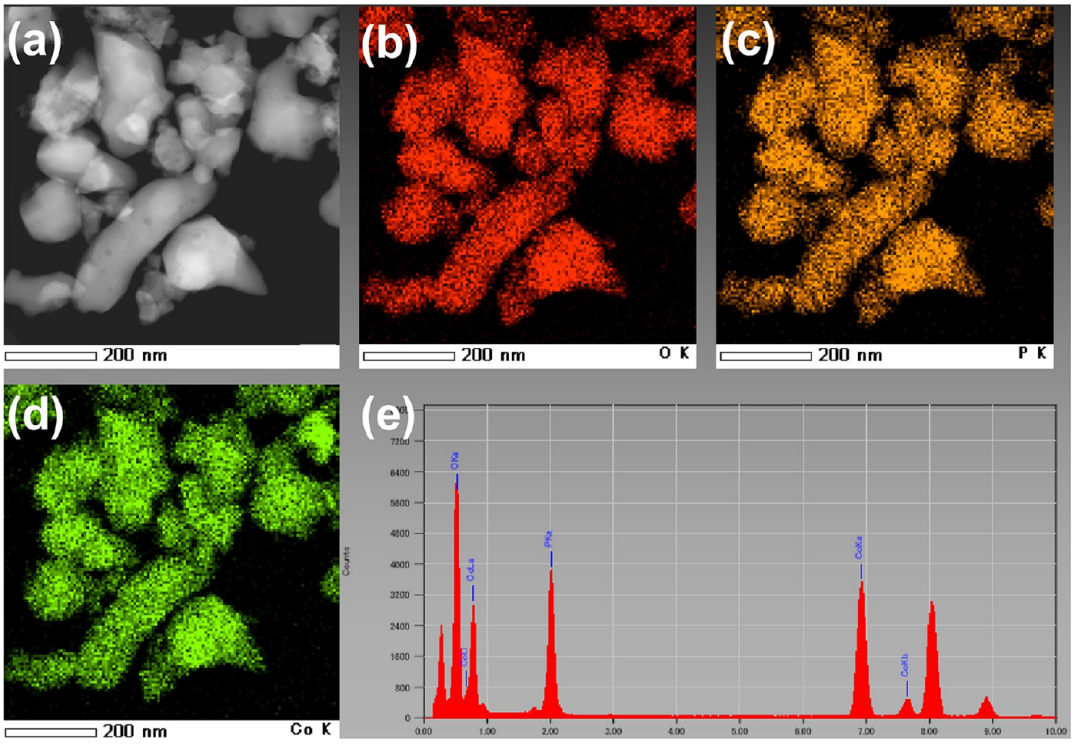

Figure 6. (a) STEM image, (b–d) elemental mapping, and (e) EDS spectrum of the synthesized $LiCoPO_4$ particles determined by STEM analysis.

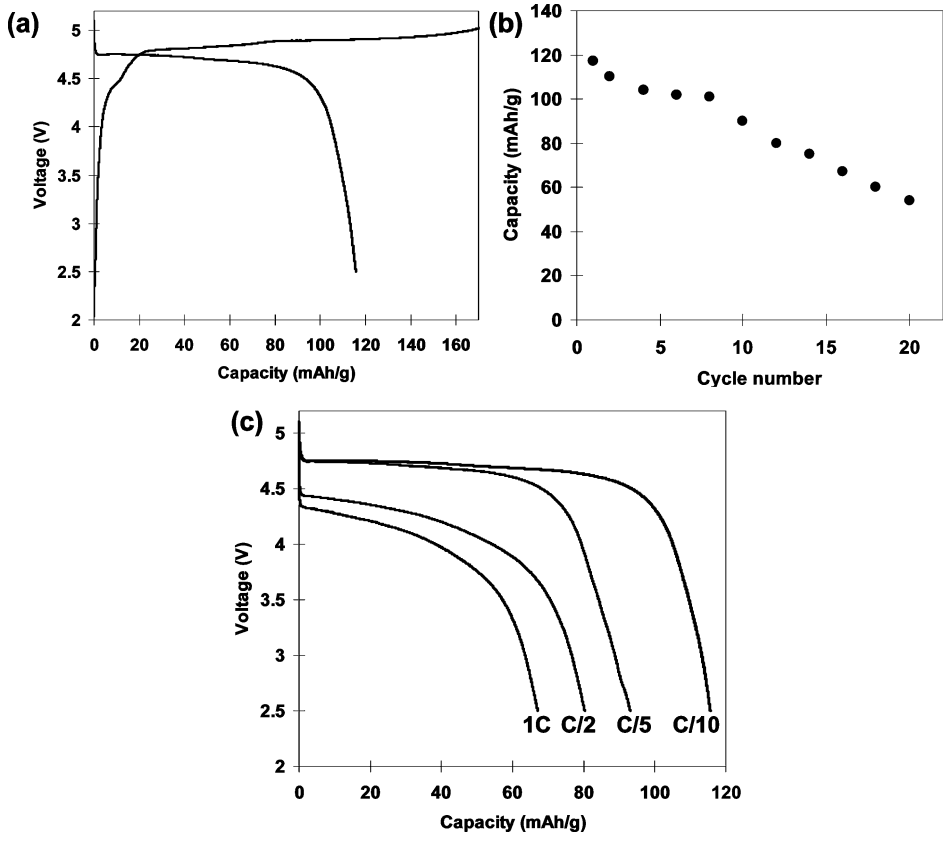

Figure 7. Electrochemical performance of the synthesized $LiCoPO_4$ in Li-ion batteries tested in the potential range of 2.5–5.1 V: (a) typical first charge–discharge profiles, (b) cyclic performance of $LiCoPO_4$ at a 0.1 C rate, and (c) initial discharge curves of $LiCoPO_4$ at different currents.

observed from TEM images that the synthesized samples were the $LiCoPO_4$ particles comprised of highly crystalline particles 100–300 nm in size. The atom-by-atom olivine $LiCoPO_4$ structure was clearly visualized using HAADF and ABF STEM with observation of Li-to-Co antisite exchange defects. The $LiCoPO_4$ particles were used as cathode materials for lithium

dx.doi.org/10.1021/am403018n | ACS Appl. Mater. Interfaces 2013, 5, 9926–9932

batteries, and the cells exhibited initial discharge capacities of 117, 93, 80, and 67 mAh/g at 0.1, 0.2, 0.5, and 1 C, respectively. The low discharge capacity of the obtained material is presumably due to the occupation of Li sites by Co atoms, which blocks the Li diffusion pathway. We believe that the $LiCoPO_4$ material may have good potential for practical application if the antisite defects can be controlled and a more stable electrolyte at high voltages can be developed. Our structural analysis demonstrates an initial step in understanding the lithium storage mechanism in high-voltage $LiCoPO_4$ cathode material. Further work would include the investigation on the charge−discharge behavior and transportation mechanism of Li inside $LiCoPO_4$ material as well as the capacity fading of this cathode material.

■ ASSOCIATED CONTENT

Supporting Information

EDS spectrum and EDS maps of C, Co, P, and O determined by SEM and cyclic voltammograms of the cell containing $LiCoPO_4$. This material is available free of charge via the Internet at http://pubs.acs.org.

■ AUTHOR INFORMATION

Corresponding Authors

*Telephone and fax: 81-22-217 5815. E-mail: tqduc@mail.tagen.tohoku.ac.jp.

*E-mail: i.honma@tagen.tohoku.ac.jp.

Author Contributions

Q.D.T. and M.K.D. contributed equally to this work.

Notes

The authors declare no competing financial interest.

■ ACKNOWLEDGMENTS

This research was financially supported by the Department of New Energy and Industrial Technology Development Organization (NEDO). Q.D.T. acknowledges the Japan Society for the Promotion of Science (JSPS) for a fellowship. We thank Prof. M. Kakihana, Dr. H. Kato, and Dr. M. Kobayashi (Tohoku University) for their kind help during this research.

■ REFERENCES

(1) Devaraju, M. K.; Honma, I. *Adv. Energy Mater.* **2012**, *2*, 284−297.

(2) Dinesh, R.; Devaraju, M. K.; Tomai, T.; Unemoto, A.; Honma, I. *Nano Lett.* **2012**, *12*, 1146−1151.

(3) Amine, K.; Yasuda, H.; Yamachi, M. *Electrochem. Solid-State Lett.* **2000**, *3*, 178−179.

(4) Okada, S.; Sawa, S.; Uebou, Y.; Egashira, M.; Yamaki, J.; Tabuchi, M.; Kobayashi, H.; Fukumi, H.; Kageyama, H. *Electrochemistry* **2003**, *71*, 1136−1138.

(5) Tadanaga, K.; Mizuno, F.; Hayashi, A.; Minami, T.; Tatsumisago, M. *Electrochemistry* **2003**, *71*, 1192−1195.

(6) West, W. C.; Whitacre, J. F.; Ratnakumar, B. V. *J. Electrochem. Soc.* **2003**, *150*, A1660−A1666.

(7) Lloris, J. M.; Vicente, C. P.; Tirado, J. R. *Electrochem. Solid-State Lett.* **2002**, *5*, A234−A237.

(8) Koleva, V.; Zhecheva, E.; Stoyanova, R. *Eur. J. Inorg. Chem.* **2010**, *26*, 4091−4099.

(9) Lee, H.; Gyu, K. M.; Cho, J. *Electrochem. Commun.* **2007**, *9*, 149−154.

(10) Shui, J. L.; Yu, Y.; Yang, X. F.; Chen, C. H. *Electrochem. Commun.* **2006**, *8*, 1087−1091.

(11) Devaraju, M. K.; Dinesh, R.; Honma, I. *Electrochim. Acta* **2012**, *85*, 548−553.

(12) Wang, F.; Yang, J.; Nuli, Y.; Wang, J. L. *J. Power Sources* **2011**, *196*, 4806−4810.

(13) Liu, J.; Conry, T. E.; Song, X. Y.; Yang, L.; Doeff, M. M.; Richardson, T. J. *J. Mater. Chem.* **2011**, *21*, 9984−9987.

(14) Doan, T. N. L.; Taniguchi, I. *J. Power Sources* **2011**, *196*, 5679−5684.

(15) Wolfenstine, J.; Allen, J. *J. Power Sources* **2004**, *136*, 150−153.

(16) Han, D. W.; Kang, Y. M.; Yin, R. Z.; Song, M. S.; Kwon, H. S. *Electrochem. Commun.* **2009**, *11*, 137−140.

(17) Wang, F.; Yang, J.; Nuli, Y.; Wang, J. *J. Power Sources* **2010**, *195*, 6884−6887.

(18) Muraliganth, T.; Manthiram, A. *J. Phys. Chem. C* **2010**, *114*, 15530−15540.

(19) Murugan, A. V.; Muraliganth, T.; Ferreira, P. J.; Manthiram, A. *Inorg. Chem.* **2009**, *48*, 946−952.

(20) Kikkawa, J.; Akita, T.; Tabuchi, M.; Shikano, M.; Tatsumi, K.; Kohyama, M. *Electrochem. Solid-State Lett.* **2008**, *11*, A183−A186.

(21) Kikkawa, J.; Akita, T.; Tabuchi, M.; Shikano, M.; Tatsumi, K.; Kohyama, M. *Appl. Phys. Lett.* **2007**, *91*, 054103.

(22) Chung, S. Y.; Choi, S. Y.; Yamamoto, T.; Ikuhara, Y. *Phys. Rev. Lett.* **2008**, *100*, 125502.

(23) Chung, S. Y.; Choi, S. Y.; Yamamoto, T.; Ikuhara, Y. *Angew. Chem., Int. Ed.* **2009**, *48*, 543−546.

(24) Chung, S. Y.; Choi, S. Y.; Lee, S. S.; Ikuhara, Y. *Phys. Rev. Lett.* **2012**, *108*, 195501.

(25) Findlay, S. D.; Shibata, N.; Sawada, H.; Okunishi, E.; Kondo, Y.; Yamamoto, T.; Ikuhara, Y. *Appl. Phys. Lett.* **2009**, *95*, 191913.

(26) Findlay, S. D.; Shibata, N.; Sawada, H.; Okunishi, E.; Kondo, Y.; Ikuhara, Y. *Ultramicroscopy* **2010**, *110*, 903−923.

(27) Huang, R.; Ikuhara, Y. *Curr. Opin. Solid State Mater. Sci.* **2011**, *16*, 31.

(28) Huang, R.; Ikuhara, Y. H.; Mizoguchi, T.; Findlay, S. D.; Kuwabara, A.; Fisher, C. A. J.; Moriwake, H.; Oki, H.; Hirayama, T.; Ikuhara, Y. *Angew. Chem., Int. Ed.* **2011**, *50*, 3053−3057.

(29) Huang, R.; Ikuhara, Y. H.; Mizoguchi, T.; Findlay, S. D.; Kuwabara, A.; Fisher, C. A. J.; Moriwake, H.; Oki, H.; Hirayama, T.; Ikuhara, Y. *Appl. Phys. Lett.* **2011**, *98*, 051913.

(30) Gu, L.; Zhu, C.; Li, H.; Yu, Y.; Li, C.; Tsukimoo, S.; Maier, J.; Ikuhara, Y. *J. Am. Chem. Soc.* **2011**, *133*, 4661−4663.

(31) Lu, X.; Sun, Y.; Jian, Z.; He, X.; Gu, L.; Hu, Y. S.; Li, H.; Wang, Z.; Chen, W.; Duan, X.; Li, C.; Maier, J.; Tsukimoo, S.; Ikuhara, Y. *Nano Lett.* **2012**, *12*, 6192−6197.

(32) Lu, X.; Jian, Z. L.; Fang, Z.; Gu, L.; Hu, Y. S.; Chen, W.; Wang, Z. X.; Chen, L. Q. *Energy Environ. Sci.* **2011**, *4*, 2638−2644.

(33) Lu, X.; Zhao, L.; He, X. Q.; Xiao, R. J.; Gu, L.; Hu, Y.-S.; Li, H.; Wang, Z. X.; Duan, X. F.; Chen, L. Q.; Maier, J.; Ikuhara, Y. *Adv. Mater.* **2012**, *24*, 3233−3238.

(34) Sun, Y.; Zhao, L.; Pan, H.; Lu, X.; Gu, L.; Hu, Y.-S.; Li, H.; Armand, M.; Ikuhara, Y.; Chen, L. Q.; Huang, X. *Nat. Commun.* **2013**, *4*, 1870−1879.

(35) Devaraju, M. K.; Truong, Q. D.; Honma, I. *RSC Adv.* **2013**, DOI: 10.1039/C3RA42540A.

(36) Wang, D.; Wang, Z.; Huang, X.; Chen, L. *J. Power Sources* **2005**, *146*, 580−583.

(37) Han, D. W.; Kang, Y. M.; Yin, R. Z.; Song, M. S.; Kwon, H. S. *Electrochem. Commun.* **2009**, *11*, 137−140.

(38) Ehrenberg, H.; Bramnik, N. N.; Senyshyn, A.; Fuess, H. *Solid State Sci.* **2009**, *11*, 18−23.

(39) Sahnmukaraj, D.; Murugan, R. *Ionics* **2004**, *10*, 88−92.

(40) Saint-Martin, R.; Franger, S. *J. Cryst. Growth* **2008**, *310*, 861−864.

(41) Gardiner, G. R.; Islam, M. S. *Chem. Mater.* **2010**, *22*, 1242−1248.

(42) Liu, J. L.; Jiang, R. R.; Wang, X. Y.; Huang, T.; Yu, A. S. *J. Power Sources* **2009**, *194*, 536−540.

(43) Kuss, C.; Liang, G. X.; Schougaard, S. B. *J. Mater. Chem.* **2012**, *22*, 24889−24893.

(44) Hoang, K.; Johannes, M. *Chem. Mater.* **2011**, *23*, 3003−3013.

(45) Malik, R.; Burch, D.; Bazant, M.; Ceder, G. *Nano Lett.* **2010**, *10*, 4123−4127.

(46) Jensen, K. M. O.; Christensen, M.; Gunnlaugsson, H. P.; Lock, N.; Bøjesen, E. D.; Proffen, T.; Iversen, B. B. *Chem. Mater.* **2013**, *25*, 2282−2290.
(47) Morgan, D.; Van der Ven, A.; Ceder, G. *Electrochem. Solid-State Lett.* **2004**, *7*, A30.
(48) Chen, G.; Song, X.; Richardson, T. J. *Electrochem. Solid-State Lett.* **2006**, *9*, A295.
(49) Nishimura, S.-I.; Kobayashi, G.; Ohoyama, K.; Kanno, R.; Yashima, M.; Yamada, A. *Nat. Mater.* **2008**, *7*, 707.
(50) Chen, J. J.; Whittingham, M. S. *Electrochem. Commun.* **2006**, *8*, 855−858.
(51) Chen, J. J.; Graetz, J. *ACS Appl. Mater. Interfaces* **2011**, *3*, 1380−1384.
(52) Kang, Y. M.; Kim, Y. I.; Oh, M. W.; Yin, R. Z.; Lee, Y.; Han, D. W.; Kwon, H. S.; Kim, J. H.; Ramanath, G. *Energy Environ. Sci.* **2011**, *4*, 4978−4983.
(53) Nakayama, M.; Goto, S.; Uchimoto, Y.; Wakihara, M.; Kitajima, Y. *Chem. Mater.* **2004**, *16*, 3399−3401.
(54) Bramnik, N. N.; Bramnik, K. G.; Baehtz, C.; Ehrenberg, H. *J. Power Sources* **2005**, *145*, 74−81.
(55) Bramnik, N. N.; Nikolowski, K.; Baehtz, C.; Bramnik, K. G.; Ehrenberg, H. *Chem. Mater.* **2007**, *19*, 908−915.